RNA promotes synapsin coacervation and modulates local translation

Branislava Rankovic[1,2,#], Zachary M Geisterfer[2,3,#], Akshita Chhabra[1,2,§] , Vladimir M Jovanovic[4,§], Ian Seim[3,8,§], Christian Hoffmann[1,2,§], Antonela Condric[1], Gerard Aguilar Pérez[1], Kiara Freitag[5], Katja Nowick[4], Marina Jendrach[5], Frank Heppner[5], Sofiia Reshetniak[6], Amy S Gladfelter[2,3,*], Dragomir Milovanovic[1,2,7,*]

1 Laboratory of Molecular Neuroscience, German Center for Neurodegenerative Diseases (DZNE), 10117 Berlin, Germany
2 Whitman Center, Marine Biological Laboratory, 02543 Woods Hole, MA, USA
3 Department of Cell Biology, Duke University, Durham, North Carolina 27708, USA
4 Human Biology and Primate Evolution, Freie Universität Berlin, 14195 Berlin, Germany
5 Department of Neuropathology, Charité - Universitätsmedizin Berlin, corporate member of Freie Universität Berlin, Humboldt-Universität zu Berlin and Berlin Institute of Health, 10117 Berlin, Germany.
6 Institute for Neuro- and Sensory Physiology, University Medical Center Göttingen, 37073, Göttingen, Germany
7 Einstein Center for Neuroscience, Charité-Universitätsmedizin Berlin, Corporate Member of Freie Universität Berlin, Humboldt-Universität Berlin, and Berlin Institute of Health, 10117 Berlin, Germany
8 Present address: Max Planck Institute for Molecular Cell Biology and Genetics, 01307 Dresden, Germany

# These authors contributed equally.
§ These authors contributed equally.
* Correspondence to: amy.gladfelter@duke.edu; dragomir.milovanovic@dzne.de

Abstract

Condensates are found at synapses where they support the clustering of synaptic vesicles (SVs) and neurotransmitter release. The possibility of RNA promoting the formation or function of these condensates is not known. Here, we set out to assess whether RNA affects molecular condensates in the synapse or could be regulated at these sites, focusing on synapsin-1, which is essential for synapse condensates. Using *in vitro* reconstitution systems, cell lines and neurons, we show that RNA drives synapsin-1 coacervation, with some bias toward structured RNAs being more effective at promoting demixing. The importance of RNA was confirmed in living synapses, where acute disruption of native RNA induces a dispersion of SVs and synapsin. Conversely, ectopically expressed SV-like condensates have the ability to recruit RNA species and the translational machinery, which accumulates within condensate-microdomains, resulting in increased translation efficacy. Our work indicates a novel role of RNAs in modulating SV condensates, as well as translation, at the synapse.

Key Conclusions

- **RNA forms coacervates with synapsin-1 that readily sequester SVs.**
- **Acute disruption of RNA affects the organization of the presynapse.**
- **RNA secondary structure tunes the assembly of synapsin-SV condensates.**
- **RNA competes with α-synuclein for partitioning at the condensates.**
- **Synapsin-1/RNA condensates are hubs for local translation.**

Introduction

Brain functioning critically relies on efficient neuronal communication. This is achieved via defined compartments—synapses, where chemical neurotransmitters are released from presynaptic axonal boutons to postsynaptic terminals of a dendrite[1]. As highly polarized, long-living and non-dividing cells, neurons require constant remodeling of the local proteome, which is tightly controlled in a spatial and temporal manner[2,3]. In response to environmental cues, protein synthesis occurs in soma[4,5,6], dendrites[7,8] and axons[9,10,11,12] including pre- and post- synapse[13,14,15], axonal growth cones[16,17] and on moving membranous organelles such as late endosomes and lysosomes[18,19].

For effective local translation, mRNA molecules and translational regulators are packaged into RNA granules, membrane-less compartments that form by the biomolecular condensation of proteins and nucleic acids[20,21]. This form of organization allows for the coordinated transport to and translation of mRNAs at designated locations in the cell[22,23,24]. The failure in assembly and trafficking of RNA condensates in implicated in neurodegenerative diseases[25,26,27,28,29].

Despite the clear relevance of targeted mRNA trafficking and the controlled local translation in axons, several crucial questions about spatial control of translation remain open. How are presynaptic RNAs, ribosomes, and translational components sequestered and maintained within the presynaptic boutons? What is the impact of RNAs and translation machinery on the organization of presynaptic boutons, in particular the cluster of synaptic vesicles (SVs), a defining feature of presynapse and an example of biomolecular condensate composed of hundreds of SVs[30]? Finally, it is unclear whether the crowded environment of presynapse is permissive for an augmented local translation.

Here, we discover that synapsin phase separates with RNAs and that synapsin/RNA condensates sequester SVs. Interestingly, the secondary structure and length of both non-coding[31,32] and messenger (m)RNAs[33,34,35] modulate assemblies of RNA granules. In support of our observation, we identify an RNAome of ectopically-generated SV-like condensates. By establishing opto-chemical manipulations in living neurons, we further show that the acute disruption of RNAs *in situ* disperses SVs from the boutons. Moreover, by adapting an *ex situ* translation assay, we show that synapsin condensates enhance the translational capacity of client mRNAs, further supporting biomolecular condensates as both attenuators and activators of translation[36,37,38]. Together, our work provides evidence of a role for RNAs in modulating SV condensates and RNA metabolism at the synapse.

Results

RNA promotes the biomolecular condensation of synapsin-1

Biomolecular condensation can be driven through interactions between oppositely charged molecules, a process known as complex coacervation[39]. As one of the most abundant, highly charged proteins (pI 12.4) in the presynapse[40], we were interested to see if synapsin-1 could undergo biomolecular condensation with RNA (**Fig. 1a**). We incubated recombinant EGFP-tagged synapsin-1 (hereafter referred to as synapsin) and total neuronal RNA across a range of concentrations. Importantly, these mixtures did not include any additional molecular crowder. Indeed, we observed that synapsin-1 was able to undergo phase separation *in vitro* in the presence of RNA (**Fig. 1b, c and Extended Data Fig. 1**). Similar to previously reported synapsin-1 homotypic protein condensates[41], these synapsin-1/RNA condensates are dynamic, and show a 65 % recovery of mobile fraction within minutes after photobleaching (**Fig. 1c**). In

addition, these RNA-driven synapsin-1 condensates retained their property to recruit SVs into their phases (**Extended Data Fig. 2**). To assess if the synapsin condensates require neuronal RNA to be maintained (**Fig. 1b, c**), we added RNase A upon formation of synapsin-1/RNA condensates and followed its effect on the condensates over the course of 10 min (see Methods) (**Fig. 1d, Extended Data Fig. 3a, b**). Upon RNase A treatment, we observed a decrease of synapsin-1 signal within the condensates, and in some cases, the complete dissolution of condensates (**Fig. 1d,** RNase A 1 μg/μl treatment). This effect was dose dependent, with concentrations as low as 0.1 μg/μl capable of reducing synapsin-1 partitioning to condensates (**Fig. 1d, e**). Similarly, RNA pre-digested with RNase A was incapable of supporting the condensation of synapsin-1 (**Extended Data Fig. 3c**) indicating the polymeric form of RNA is required. These results suggest that RNA, in the absence of molecular crowders can promote the condensation of synapsin-1 *in vitro*, as synapsin-1 alone would not form condensates without RNA or crowders[41,42].

RNA structure modulates the stoichiometry of RNA and synapsin-1 within condensates

Recent evidence suggests RNA structure, in addition to charge and primary sequence, can control the formation and specificity of protein-RNA condensates[35,43,44]. To understand the contribution of RNA structure in the formation of synapsin condensates, we utilized an orthogonal mRNA, *CLN3*, designed *in silico* to either sample many different conformations akin to an IDR (high ensemble diversity, called *CLN3* high-ED) or sample relatively few different conformations (low ensemble diversity, called *CLN3* low-ED), while preserving the total nucleic acid content and length[45]. Two sequences were chosen representing these different classes of conformational heterogeneity based on their minimum free energy (MFE) and ensemble diversity (ED) (**Fig. 2a**)[46,47]. These RNAs were added to reactions containing synapsin-1 in a 1:1 polyelectrolyte charge ratio and allowed to form condensates. For both *CLN3* structure mutant systems, we saw the immediate formation of synapsin-1/RNA condensates (**Fig. 2a**). Notably, the partitioning of synapsin-1 to the condensates varied based on RNA structure (**Fig. 2b**). Condensates formed with RNAs that have low conformational heterogeneity (*CLN3* low-ED) tended to be more protein-rich, as opposed to condensates formed in the presence of RNAs with more diversity in possible structures (*CLN3* high-ED). (**Fig. 2b**). While full-length synapsin-1 was able to form condensates with both kinds of RNAs, the synapsin-1 IDR (421-705) was only able to form condensates with more conformationally heterogeneous RNAs (**Extended Data Fig. 4**). These results suggest that RNA structure heterogeneity, in addition to charge, is an important feature in regulating the formation of synapsin-1/RNA condensates.

Each presynapse contains over 300,000 protein copy numbers[40], among which the most abundant is synapsin-1. α-Synuclein, another abundant protein in the presynapse that regulates the formation and stoichiometry of synapsin-1 condensates[48], is a highly acidic and negatively charged protein (pI = -9.73 at pH 7.4)[49]. We hypothesized that RNA and α-synuclein may compete in their recruitment to synapsin-1 condensates based on their negative charge. To understand how the presence of multiple different anionic polymeric molecules might affect synapsin-1 condensation *in vitro*, we first pre-formed α-synuclein/synapsin-1 condensates at their physiological stoichiometry[40]. Once the condensates were formed, *CLN3* high-ED or *CLN3* low-ED were added to the reactions and the subsequent shifts in the partitioning of synapsin-1 and α-synuclein were measured. Upon the addition of either *CLN3* high-ED or low-ED, the RNA was recruited into pre-existing α-synuclein/synapsin-1 condensates, in addition to forming synapsin-1/RNA condensates devoid of α-synuclein (**Fig. 2c, d and Extended Data Fig. 5**), which suggested both negatively charged molecules, RNA and α-synuclein, can regulate formation and stoichiometries of synapsin condensates *in vitro*.

To further understand the impact of RNA on the association of synapsin-1 and α-synuclein, we analyzed the stoichiometry of synapsin-1 and α-synuclein within condensates, calculated as a ratio of intensities of synapsin-1 to α-synuclein before and after the addition of RNA to the reactions (**Fig. 2e**). After the addition of either *CLN3* high- or low- ED, we observed a disruption in the ratio of synapsin/α-synuclein concentrations within synapsin condensates. Such differential enrichments of synapsin and α-synuclein after the addition of RNA suggests that the availability and regulation of RNA in the presynapse may be an important determinant of synapsin condensate stoichiometry in both healthy and disease states.

RNA conformational heterogeneity is persistent across purified synapsin-1 condensates

Given that we see RNA has potent effects on synapsin condensates, we set out to identify the RNAs than can associate with synapsin-1. To address this, we ectopically expressed SV-like condensates of specific identities in a HEK293 cell line, a system conducive to downstream subcellular fractionation and condensate isolation. Cells expressed either mCherry-synapsin-1 alone, or mCherry-synapsin-1 and α-synuclein (**Fig. 3a, b**). In both cell lines, condensation of synapsin-1 (or synapsin-1 and α-synuclein) was promoted by simultaneous co-expression of the synaptic vesicle protein, synaptophysin[50]. For each condition, SV-like condensates were purified from cells lines using a previously established protocol for RNP condensate purification[51] (**Fig. 3a, Extended Data Fig. 6**). RNA purified from the two SV-like condensates was subsequently submitted for high-throughput RNA sequencing (see Methods). Differential enrichment analysis of the two condensate forming conditions showed largely distinct RNA content for each condition (**Fig. 3c, Supplementary Table 7**), with 116 transcripts enriched in synapsin-1 only condensates, as opposed to 203 transcripts enriched in synapsin-1 and α-synuclein condensates (**Fig. 3c)**. These results suggest that synapsin condensates can readily recruit a diverse range of RNA species when expressed in HEK293 cells, prompting us to assess what features of these RNAs led to their recruitment.

Although the precise molecular identify of these RNAs differed between the two conditions, we were first interested in identifying potential sequence elements, or motifs, that may be over-represented amongst the two populations of RNAs. To search for over-represented sequence motifs, we performed MEME analysis[52] on the purified SV-like transcriptomes. Limiting occurrences of motif elements to either zero, or once per transcript, we were able to identify short sequence elements for both transcriptomes whose frequency amongst the RNAs was unlikely given random chance (**Extended Data Fig. 7a, b**). Importantly, these sequence elements are high in G-content and often contain GGGAG motifs within them, suggesting these regions may form higher order structures such as G-quadruplexes[53]. Additionally, the similarity in nucleotide composition of these sequence elements, despite differences in RNA identity between the two transcriptomes, suggests these ectopically expressed condensates may favor the inclusion of RNAs with more stable secondary structure[54].

To further investigate the RNA structural heterogeneity associated with these transcriptomes, we predicted the ED values for RNAs enriched in SV-like condensates and plotted these values as a function of RNA length (**Fig. 3d**). Both transcriptomes (with or without co-expression of α-synuclein) were enriched in shorter RNAs with less structural heterogeneity (low-ED) (**Fig 3c**), in agreeance with what we observed at the individual sequence level (**Extended Data Fig. 7f,g**). Notably, this moderate bias towards short, low-ED RNA is specific to RNAs associating with synapsin/SV-like condensates and not an attribute of the human kidney transcriptome (see also *Ashbya gossypii* and synaptic transcriptome**, Extended Data Fig. 7c-f**)[55]. An analysis of the length-normalized ED (NED) of a few different transcriptomes shows

that the SV-like condensates have a lower NED compared to the other datasets (**Extended Data Fig. 7g**). This observation is consistent with the *in vitro* data in which the *CLN3* low-ED mutant recruits more synapsin (**Fig. 2b**). Furthermore, the preferential recruitment of low-ED RNAs could be explained by low-ED RNAs having lower entropic cost of demixing because they experience less of a conformational entropy penalty[45]. This result suggested to us that synapsin-1 condensates may have preferences for properties of RNA, such as structure, and that inclusion of these RNAs may not be solely by electrostatics, as the electrostatics alone would favor the inclusion of longer RNAs due to their reduced entropic cost of association[56].

Given the clear impact of RNA conformational heterogeneity in driving the stoichiometry of RNA and protein within synapsin-1 condensates with orthogonal RNAs (**Fig 2**), we were interested to see whether native synaptic mRNAs of differing structure produce the same effect. To investigate this, we selected two synaptic mRNAs, *Scg3* and *Prnp* from the recently determined transcriptome from mouse primary neurons[57] with identical lengths but different structural features ($Scg3_{ED}$=435, $Prnp_{ED}$=635) (indicated in **Extended Data Fig. 8**). We pre-formed protein only condensates containing α-synuclein and synapsin-1 to a final protein concentration ratio, mimicking near-physiological conditions (**Fig. 4a**). After formation of protein-only condensates, *Scg3* or *Prnp* were added to the reactions in a 1:1 polyelectrolyte charge ratio (based on the charge and abundance of synapsin-1) and partitioning of each molecule was analyzed (**Fig. 4b**). RNA recruitment was observed within a few minutes after their addition to the reaction (**Extended Data Fig. 9a-d**), followed by the recruitment of synapsin-1 but no compensatory recruitment of α-synuclein (**Fig. 4c**), in agreeance with what was observed for the reconstitutions with model RNAs (**Fig. 2c-e**).

The rapid and continued recruitment of RNA to preformed synapsin/α-synuclein condensates (**Fig 4b**) prompted us to investigate how readily α-synuclein could be recruited to preformed synapsin-RNA condensates. After preforming synapsin-RNA condensates and supplementing reactions with α-synuclein (**Fig. 4d**), we measured α-synuclein recruitment into synapsin-1/RNA condensates at two different time points (**Fig. 4d, e**). Despite seeing an initial, moderate recruitment of α-synuclein to synapsin-1/RNA condensates, no additional enrichment was observed in the course of incubation time. This is in contrast to synapsin-1 and RNA, which continued recruitment to preformed synapsin-1/RNA condensates over the two time points measured (**Extended Data Fig. 9e, f**). Interestingly, the difference in structural heterogeneity between these RNAs was insufficient to drive significant differences in the amount of synapsin recruited to condensates (**Extended Data Fig. 10**), as was observed with the *CLN3* RNAs (**Fig. 2b**). It is important to note that in addition to differences in the magnitude of structural heterogeneity between the two RNA systems (*CLN3* ED range = 114 – 627; Prnp/Scg3 ED range = 435 – 635), there are notable length differences (*CLN3* = 1588 nt; Prnp/Scg3 = 2193 nt) that contribute to outcome of these reactions. Furthermore, these reactions were only carried out in a 1:1 charge ratio, which results in the same ratio of synapsin to nucleotide content between the two systems, but results in different numbers of RNA molecules per reaction, with *Scg3* and *Prnp* reactions containing less RNAs. Taken altogether, these results suggest RNA can be a potent factor in modulating condensation of synapsin-1 in a minimal system.

The acute RNA disruption causes a dispersion of synaptic vesicles in living neurons

After observing synapsin-1/RNA condensation *in vitro*, we wanted to know whether the loss of RNA could lead to the depletion of synapsin-1 condensates at the presynapse of primary hippocampal neurons. To promote the uptake of RNase A into neurites we employed an approach based on photochemical internalization (PCI) system[58,59], modified in a way to prevent damage to recycling organelles (**Fig. 5a, Extended Data Fig. 11**). After PCI-mediated

membrane permeabilization, 150 µg/ml of RNase A, or BSA as a control, was supplemented to WT rat neuronal cultures co-expressing EGFP-synaptophysin (Syp) and mScarlet-synapsin-1 (Syn 1). We then measured the fluorescence intensity and distribution of synaptophysin and synapsin-1 at synaptic boutons (**Fig. 5b, Extended Data Fig. 12a, c**). We observed a significant decrease of fluorescent signal of both proteins, as well as their dispersion from the synaptic boutons (**Fig. 5c, d**). As opposed to RNase A treatment, no effect was observed when neurons were incubated with BSA (**Fig. 5e-g, Extended Data Fig. 12b**), indicating the importance of RNA molecules for synaptophysin and synapsin-1 enrichment at the presynapse. Together, these results in live neurons clearly demonstrate that synapsin-1 enrichment at the presynapse is dependent on RNA.

Synapsin-1 condensates harbor mRNA translational machinery components

Our results so far suggest RNA as a potential scaffold, for the promotion and or stabilization of synapsin-1 condensates both *in vitro* and primary neurons. We next went on to assess if being sequestered into a synapsin-1 condensate influenced the translation of the mRNA. We hypothesized that biomolecular condensation of synapsin-1 may function in organizing local protein synthesis at the presynapse, in addition to organizing SVs. This would provide an additional mechanism by which neurons regulate local protein synthesis, a critical feature of these large and highly polarized cells. To test if there is a role of synapsin-1 in regulating translation, we first wanted to validate the presence of mRNA molecules at the synaptic region of our mouse primary neuronal culture. To visualize mRNA at the presynapse, we used fluorescent in situ hybridization (FISH) directed towards the poly(A) tail of mRNA at DIV14. We observed an obvious enrichment of mRNA at vGLUT1 positive foci, a presynaptic marker (**Fig. 6a, Extended Data Fig. 14a**), suggesting a local enrichment of mRNA at the presynapse. In addition, employing single molecule (sm)FISH in primary neurons we observed that highly abundant mRNA, *Atp5b*, coding for β subunit of ATP synthase[60,61] was also colocalizing with our presynaptic marker, vGLUT1 (**Fig. 6b, Extended Data Fig. 14b**). Further, for operational purposes, using the ectopically generated SV-like condensates, we wanted to test whether the translational machinery can associate with synapsin-driven condensates. Our immunocytochemistry analysis showed that eukaryotic initiation factor 4E (EIF4E), one of the components of the translational machinery, colocalizes with or at the interface of mCherry-synapsin-1 condensates (**Fig. 6c-e**). This supported our idea to further assess potential capacity of synapsin condensates to promote translation.

Synapsin-1 condensates enhance mRNA translation

To assess if the association of mRNAs with synapsin influences their translation, we first generated a luciferase reporter for one of synaptic mRNAs analyzed above *Atp5b*. In our reconstitution assays, *Atp5b* readily co-condenses with synapsin-1 when mixed in a 1:1 polyelectrolyte charge ratio (**Fig. 7a**). To measure translation in the presence of synapsin-1 condensates, we preformed synapsin-1/RNA condensates with *Atp5b* mRNA containing a 3' fusion to NanoLuciferase (Nluc). After the formation of condensates, rabbit reticulocyte extract (RRE) was added to the reaction and left to incubate at 30°C. After one hour, vivazine was added to the reactions and luminescence generated by the successful translation of *Atp5b-Nluc* was read out on the luminometer. Strikingly, mRNAs in reactions containing pre-formed synapsin-1/RNA condensates showed enhanced translation when compared to RNA only reactions, and translation could be further increased by the addition of α-synuclein to reactions (**Fig. 7b**). Importantly, this increase in translation is not a byproduct of simply crowding, as the addition of 4.5 µM BSA to reactions did not enhance translation above RNA alone. These data indicate that the presence of synapsin-1 condensates can enhance translation of mRNAs in the same reaction.

We next asked if this promotion of translation was happening within or at the synapsin condensate interface. To visualize translation events, we turned to a fluorescence-based approach called MoonTag (**Fig. 7c**)[62]. This system relies on the strong association of a fluorescently labeled nanobody (2H10Nb) with nascently translated MoonTag (gp41) peptides. By fusing a sequence coding for 24 MoonTag peptides to *Atp5b* mRNA coding sequence, we can visualize the translation of mRNAs through the accumulation of fluorescently-labeled nanobodies. As above, we pre-formed synapsin-1/RNA condensates with *Atp5b-MoonTag* mRNA and then supplemented reactions with RRE and mCherry-labeled nanobodies. The MoonTag did not change the basic conditions at which synapsin-1 to phase separates (*Atp5b-MoonTag = 3052 nt; ED = 1025)*). To our surprise, we saw large nanobody foci contained within pores within synapsin-1 condensates as well as foci on the surface (**Fig. 7c, d**). Notably, these same pores could be seen in condensates formed with *Atp5b-Nluc* when added to RRE, however the recruitment of nanobody was specific to condensates having RNAs with the MoonTag sequence, indicating that synapsin-1 condensates are not concentrating the nanobody itself (**Fig. 7d, e**).

Additionally, large dextrans readily pass through these condensates, suggesting translation machinery may also concentrate within these condensates (**Extended Data Fig. 15**). Interestingly, the average nanobody signal associated with synapsin condensates in MoonTag reactions containing α-synuclein was lower than those containing synapsin alone (**Fig. 7e**). This is in contrast to the luciferase reaction containing both synapsin and α-synuclein, which showed an increase in mRNA translation over synapsin-only conditions (**Fig. 7b**). These results would seem to suggest either that (i) MoonTag signal provides a spatial marker for where translation is occurring but the average signal per condensate is not an informative metric with regards to translation efficiency or (ii) the addition of α-synuclein leads to the differences in residency of already translated, nanobody-bound MoonTag peptides, leading to a loss of nanobody signal from synapsin condensates. Regardless of the interpretation, the increase in translation of mRNAs in reactions containing synapsin-RNA condensates (**Fig. 7b**), and the observation of translational microdomains within synapsin condensates (**Fig 7d**)), suggested to us that synapsin-1 condensates may act as translational crucibles, organizing protein synthesis in the presynapse.

Discussion

In this study, we discover that synapsin-1, a highly abundant protein in the presynapse, readily forms condensates with RNA well below the physiological concentrations of this protein. *In vitro* reconstitutions indicate increased synapsin recruitment in condensates formed with RNA with low conformational heterogeneity. Consistent with some role for RNA structure, there is a moderate bias in RNAs that associate with synapsin-1 condensates in cells to be short and have lower relative conformational heterogeneity. Disruption of RNA within the presynapse is sufficient to disperse synapsin-1 and SVs in cultured neurons. In addition to RNA playing a role in condensate formation/maintenance, we provide evidence that RNA translation may be promoted by synapsin-1 condensates.

RNA structure heterogeneity can influence synapsin-1 condensates

Synapsin-1 lacks any classical RNA binding domain (RBD); thus, it is likely that binding and condensation of synapsin and RNA is driven primarily through electrostatic interactions between the highly positively charged synapsin-1 and the negative charge of RNA[63]. Indeed, the IDR of synapsin-1, a necessary and sufficient region for its phase separation[64], was also sufficient to form condensates with RNAs, although of smaller size (**Extended Data Fig. 4**). However, in addition, our data show that differences in RNA conformational heterogeneity can alter recruitment of client proteins such as α-synuclein and impacts the concentration of both RNA and proteins in synapsin-RNA condensates (**Fig. 2**). We find that condensates formed by less conformationally heterogeneous RNAs promote greater partitioning of synapsin-1 (**Fig. 2**) and that synapsin condensates have a moderate bias towards the recruitment of less conformationally heterogeneous RNAs (NED analysis; **Extended Data Fig. 7g).** These results indicate that in addition to length and nucleotide composition, RNA structural heterogeneity may act as a knob by which neurons might tune the formation and dissolution of synaptic vesicle-containing condensates in the small volume of synaptic bouton. RNA modifications, editing and helicases could all shift the ED of a given sequence and impact the concentrations/properties of synapsin-1 condensates locally in the neuron. Furthermore, RNA itself may contribute to the composition of SV condensates in the complex milieu of the presynapse, where multiple competing interactions among proteins can occur.

α-Synuclein competes with RNA for enrichment into synapsin/SV condensates

α-Synuclein, a prominent SV cluster component, is recruited into synapsin/SV condensates[48]. Recently, α-synuclein was demonstrated to interact with few components of P-bodies, another prominent example of RNA granules. Moreover, many of these proteins are part of the decapping machinery, suggesting α-synuclein role in modulating the stability of mRNA stored therein[65]. Together, these two studies point to a direct relation between the SV cluster and mRNA processing, presumably modulated by α-synuclein. While neither α-synuclein alone nor SVs alone were sufficient to form condensates our data show that the partitioning of α-synuclein into synapsin condensates is sensitive to the presence of RNA, strongly suggesting RNAs could be both a substrate as well as competitor for interactions with synapsin-1 (**Fig. 2 and Fig. 4**). These intricate associations between proteins and RNAs could be important in the organization of the presynapse, with mis regulation of protein-RNA interactions potentially contributing to the onset or emergence of neurodegeneration[66,67].

Synapsin-1, an unconventional RNA-binding protein

While classical RBPs contain RNA-binding domains (RBDs), for unconventional RBPs (unRBPs), interactions with mRNAs are thought to be largely dominated by weak, non-sequence specific interactions, often involving the high abundance of unRBPs – all of which

386 sit in agreement with our observations for synapsin. As our reconstitution results from above
387 show that RNA structure directly influences the propensity for synapsin-1 to undergo phase
388 separation and modulates the partitioning of client proteins, we hypothesized that RNA
389 signature will be consistent for synapsin-1 condensates in cells. Indeed, our assessments of
390 synapsin-condensate transcriptomes indicate the presence of multiple RNA species. In general,
391 we observed a bias towards the inclusion of shorter RNAs with lower conformational
392 heterogeneity (**Fig. 3**). The bias for low ED RNA elements was true for synapsin condensates
393 regardless of α-synuclein presence (**Fig. 3**). In either case, these enriched RNAs lacked any
394 ontological grouping, agreeing with general observations from unRBPs, where interactions are
395 largely agnostic to RNA sequence. Synapsin appears to have a preference for low ED RNA,
396 and the ectopically-generated synapsin-1/SV-like condensates are enriched in shorter RNA
397 (e.g., a few hundred nucleotides). However, an intriguing aspect is that low ED RNAs are not
398 statistically more common in the transcriptome of adult kidney cells[55]. This suggested to us
399 that conformation less heterogeneous RNAs may lower the critical concentration of synapsin-
400 1 condensation and are therefore enriched in synapsin/SV condensates. Further studies
401 identifying the exact sequence space that synapsin-1 binds along RNA will be helpful in
402 determining the nature of synapsin-RNA interactions.
403
404 To complement our transcriptome observations from ectopically-generated synapsin
405 condensates, we probed the effect of two structurally different synaptic mRNAs (*Scg3* and
406 *Prnp*)[57] identified at the synapse on *in vitro* condensation of synapsin-1 and α-synuclein. Even
407 though we observed a clear competition between mRNAs and α-synuclein (as with orthogonal
408 mRNAs in **Fig. 2**), no difference between *Scg3* and *Prnp* synapsin-1/α-synuclein condensates
409 were observed under our experimental conditions. This can be the consequence of these two
410 transcripts having more similar ED values than the *CLN3* sequences, suggesting that more
411 extreme structural differences or specific RNA sequence motifs are required to drive
412 differential condensation into synapsin condensates. Nonetheless, we do not exclude the
413 possibility a different RNA/protein initial concentration, would reveal differences in dense
414 phase recruitment as a function of ED and/or RNA secondary structure.
415
416 **Synapsin-RNA condensates are hubs for the local translation**
417 Spatial control of translation was first implicated in neurons after the observation of preferential
418 localization of polyribosomes at the base of dendritic spines[68] reinforcing the notion that local
419 protein synthesis occurred in dendrites but not in axons or presynaptic sites. This view evolved
420 with the data demonstrating the local translation at the presynapse[69,70] . Our studies demonstrate
421 a potential role for synapsin-1 in regulating this process at the presynapse through the formation
422 of biomolecular condensates. We show that, in contrast to some ribonucleoprotein
423 condensates[71,72,73], the presence of synapsin condensates enhances translation of RNAs by
424 several orders of magnitude (**Fig. 7**). Though the mechanistic basis of this enhancement
425 remains unknown, it is possible that the positive charge of synapsin-1, thought to be the major
426 driving force in synapsin-RNA interactions, may also aid in capturing and concentrating
427 negatively charged ribosomal components or other translational machinery. Such pronounced
428 translation activity within synapsin condensate microdomains and at the interface of synapsin
429 condensates[74] may be the result of interfacial ion potential that can generate permissive
430 chemical environments[75] and necessary protein conformations[76] to facilitate effective
431 translation.
432
433 Our spatial analysis of translation in synapsin condensates support this hypothesis, as we
434 observe sub-domains within synapsin-1 condensates that show signal for active translation
435 (**Fig. 7**). Our dextran-based assessment (**Extended Data Fig. 15**) of the mesh pore size within

condensates suggests that pores are sufficiently large for translated proteins. to diffuse out of the condensate, indicating that these fluorescently-labeled Moontag nanobodies depict the 'hot spots' of active translation within the condensates. These observations build further evidence for of condensate functions beyond translational repression and RNA storage. For neurons, this translational enhancement may be particularly relevant in situations where concentrations of RNAs and ribosomal machinery are low[15]. In these scenarios, biomolecular condensation may be indispensable in ensuring RNAs are translated to the proper extent and at the right time, despite a low abundance of translational machinery.

Together, our study provides a direct insight into the architectural role of RNA in organizing the presynapse and modulating the synapsin-SV condensates distribution at the synaptic boutons. We also demonstrate that translation of mRNA can be enhanced in these presynaptic condensates, indicating the new mechanisms for coupling of SV release and local translation, as recently suggested[70]. Our study identifies the importance of RNA metabolism at the presynapse, where competing interactions among nucleic acids and proteins, such as α-synuclein, may play a critical role in regulating the spatial and temporal protein localization vital for synaptic physiology and disrupted in disease.

454 **MAIN FIGURES and FIGURE LEGENDS**
455
456
457

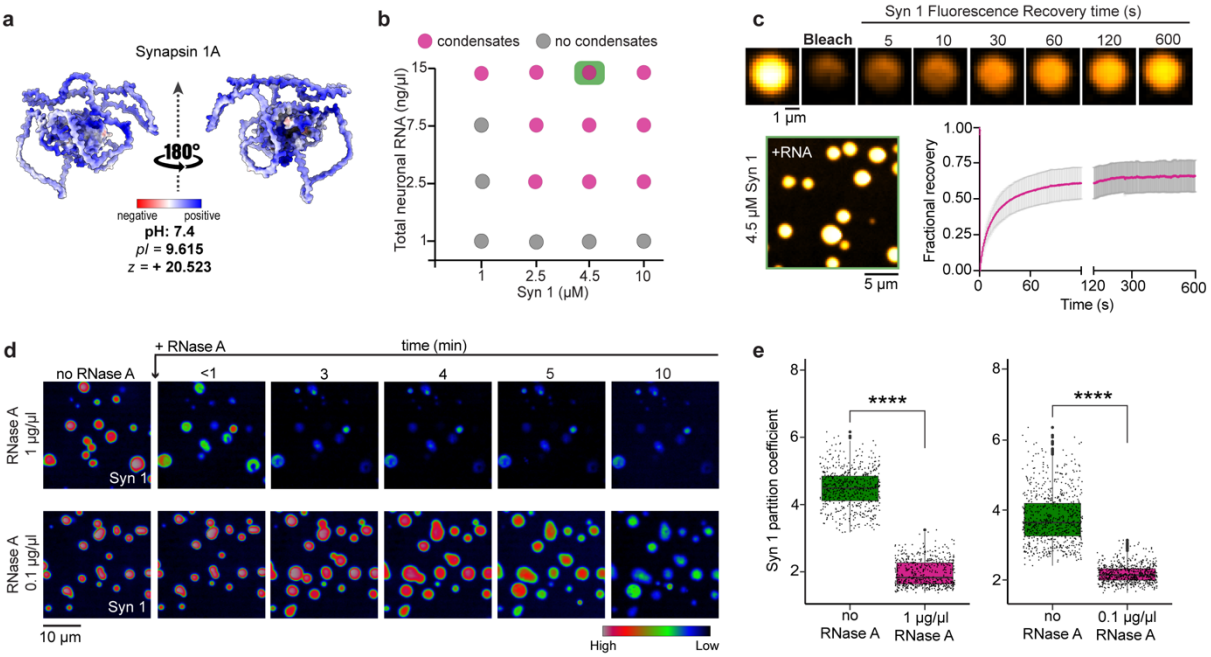

458
459
460 **Figure 1 | RNA promotes condensation of synapsin-1.**
461 **a,** Charge-based surface model of synapsin-1 (*Rattus norvegicus*; UniProt ID P00951) showing charge
462 distribution. EGFP-tagged rat synapsin-1 was purified for *in vitro* reconstitutions (further referred to as
463 Syn 1).
464 **b,** Summary of phase-separation behavior of Syn 1 in the presence of total RNA from primary mouse
465 neurons, with increasing concentrations of both protein and RNA without any molecular crowder in 10
466 µl-reaction buffer (150 mM NaCl, 25 mM Tris-HCl at pH - 7.4, 0.5 mM TCEP). Corresponding images
467 are shown in the Extended Data Fig. 1.
468 **c,** FRAP of reconstituted Syn 1 condensates (4.5 µM) with 150 ng of total neuronal RNA. Data was
469 collected from two independent *in vitro* reconstitutions. Error bars in FRAP curve plot represent
470 standard deviation (± SD). The mobile fraction of Syn 1 was 65 %. Representative images show
471 bleaching and recovery of Syn 1 fluorescence.
472 **d,** Representative images of selected RNA-driven synapsin-1 condensates treated with 1 µg/µl or 0.1
473 µg/µl final concentration of RNase A for 10 min. Fluorescence intensity signal in gray values (see
474 histogram legend) indicates fluorescence intensity signal of synapsin 1 before and at different time
475 points upon the addition of RNase A to pre-formed synapsin/RNA condensates with 10 µM Syn 1 (to a
476 final concentration) and 300 ng of total neuronal RNA.
477 **e,** Quantification of Syn 1 partition coefficient in not treated RNA-driven synapsin-1 condensates and
478 10 min after the treatment with 1 or 0.1 µg/µl of RNase A. The jitter box plot encompasses 25th and 75th
479 quartiles with median marked by central line. Minimum and maximum of quantified partition
480 coefficient are denoted by whiskers. Black circles (above the whiskers) represent quantified partition
481 coefficient outside the range of adjacent values. Each point represents the value, which was slightly
482 shifted for better visualization of overlapping data points. **** indicates $P \leq 0.0001$ by Wilcoxon rank
483 sum test. Data was collected from three independent in vitro reconstitutions.
484

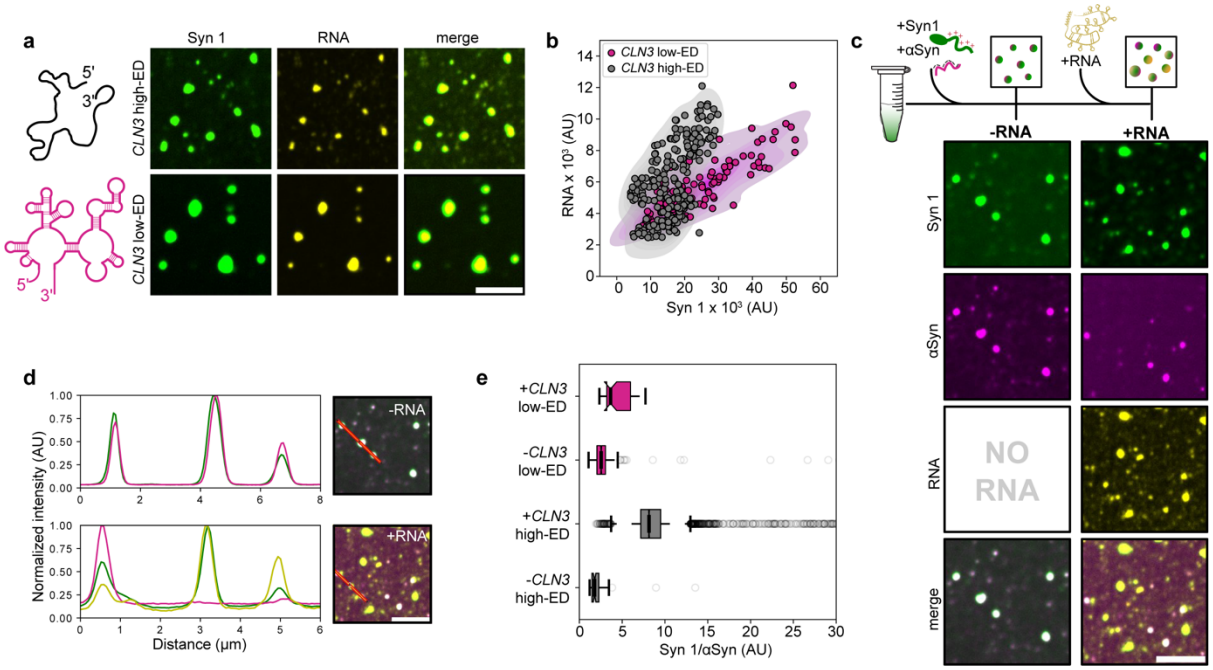

Figure 2 | RNA structure modulates the stoichiometry of synapsin-1 within condensates.
a, Representative images of *in vitro* reconstituted EGFP-synapsin-1/*CLN3* condensates with high-ED and low-ED Cy5-labelled *CLN3* mutant in the absence of molecular crowder in reaction buffer (150 mM, NaCl, 25 mM Tris-HCl (pH - 7.4), 0.5 mM TCEP). Scale bar: 10 µm.
b, Scatter plot overlayed with Kernel Density Estimate (KDE) shows fluorescence intensities of *CLN3* RNA (high-ED in grey and low-ED in magenta) as a function of EGFP-synapsin-1 (Syn 1) intensities. Each circle represents a single Syn 1/*CLN3* condensate.
c, Top: schematic representation of three-component *in vitro* reconstitution system -type I (see Methods), with purified EGFP-synapsin-1 (Syn 1), α-synuclein-AF647 (αSyn) and Cy3 labelled *CLN3* RNAs. Bottom: Representative micrographs of in vitro reconstituted synapsin-1/α-synuclein condensates without or with *CLN3* RNA. Scale bar: 10 µm.
d, Fluorescence intensity line-profiles accompanied with corresponding representative images with selected synapsin-1/α-synuclein ± *CLN3* RNA condensates used to plot the line profiles.
e, Quantifications of synapsin-1 and α-synuclein fluorescence intensities expressed as a ratio (Syn 1/αSyn) in reconstituted protein-protein droplets with or without low- or high-ED *CLN3* RNAs. The box plot encompasses the 25th and 75th quartiles with the median marked by central line. Whiskers extend to 1.5 times the interquartile range (IQR). Circles indicate outliers. A paired two-tailed T-Test comparing values before and after the addition of RNA indicate a P-value of <0.00001 and 0.00579 for high-ED and *CLN3* low-ED respectively. All data were collected from three independent *in vitro* reconstitutions.

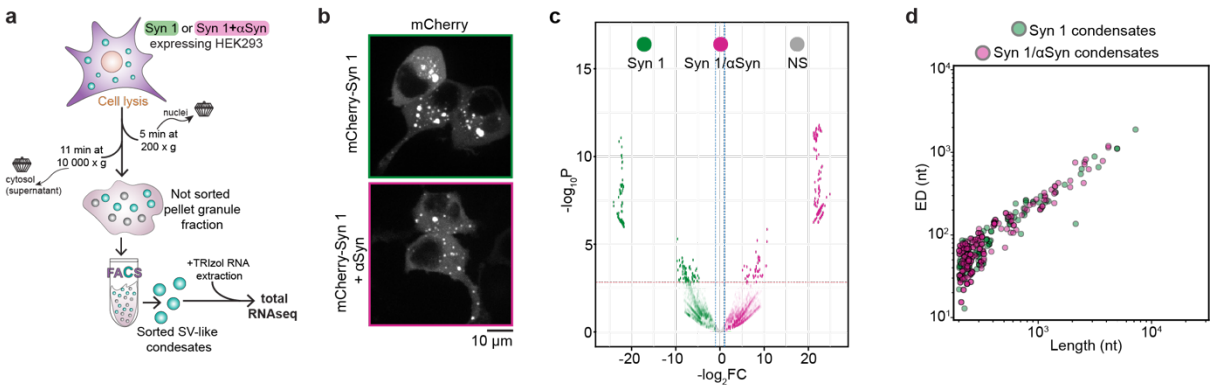

Figure 3 | RNA signature is persistent across purified synapsin-1 condensates.
a, Schematic representation of condensate purification protocol adapted from [51].
b, Representative micrographs of HEK293 cells co-transfected with mCherry-synapsin-1 and untagged synaptophysin (green, condition 1 [Syn 1 condensates]) and mCherry-synapsin-1 together with untagged α-synuclein and synaptophysin (magenta, condition 2 [Syn1/αSyn condensates]). Synaptophysin was used to promote synapsin-1 condensation *in cellulo*.
c, Volcano plot of differential expression transcriptome analysis of total RNA purified from FACS-sorted Syn 1 and Syn 1/αSyn condensates previously ectopically expressed in HEK293 cell line. The cutoff values fold change > 2 and adjusted P-value < 0.01 were utilized to identify differentially expressed transcripts. Not changed significantly (below P-value cutoff) transcripts are shown below red dotted line. Green color indicates enriched transcripts in Syn 1 condensates and magenta transcripts enriched in Syn 1/αSyn condensates. Blue dotted line indicates cutoff for fold change (FC) of transcript enrichment in condition 2 versus condition 1. NS denotes non-significant**.**
d, Ensemble diversity analysis (ED) plot of RNAs enriched in Syn 1 condensates and Syn 1/αSyn condensates. ED values (nt=nucleotides) are plotted as a function of RNA length and data was presented in $\log_{10}$ scale. Each circle in the scatter plot represents individual transcript analyzed.

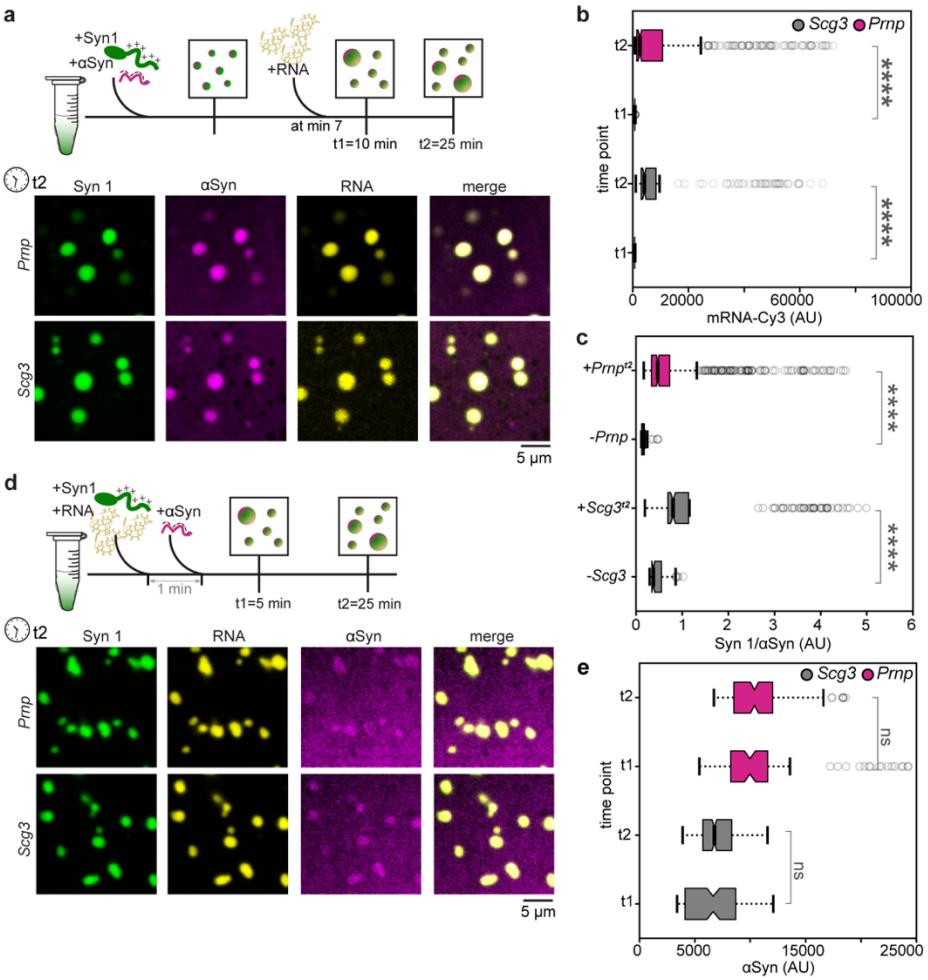

Figure 4 | Synaptic mRNAs compete out α-synuclein while maintaining the synapsin-1 stoichiometry within condensates.

a, Top: schematic representation of three-component *in vitro* reconstitution system -type I (see Methods), with purified EGFP-synapsin-1 (Syn 1), α-synuclein-AF647 (αSyn) and Cy3-labelled *Scg3* or *Prnp* RNAs. Bottom: Representative micrographs of type I *in vitro* reconstituted Syn 1/ αSyn condensates with *Scg3* or *Prnp* RNA at 25 min of incubation upon protein-protein condensate formation corresponding to 15 min post mRNA addition (t2).

b, Quantifications of RNA fluorescence intensities (*Scg3* and *Prnp*) in *in vitro* reconstituted protein-protein droplets after RNA addition (t1) and at the time point t2 (see above). Paired two-tailed T-test comparing RNA intensities at t1 to those at t2 indicates a P-value of <0.00001 (****) for both RNAs tested.

c, Quantifications of Syn 1 and αSyn fluorescence intensities expressed as a ratio (Syn 1/αSyn) in *in vitro* reconstituted protein-protein droplets without or in the presence of *Scg3* or *Prnp* RNAs 25 min after reaction set up (t2). Paired two-tailed T-test comparing the ratio of Syn1/αSyn intensities before and after the addition of RNA indicates a P-value of <0.00001 (****) for both RNAs tested.

d, Top: schematic representation of three-component *in vitro* reconstitution system type II (see Methods), with purified EGFP-Syn 1, αSyn-AF647 and Cy3-labelled *Scg3* or *Prnp* RNAs. Bottom: Representative micrographs of type II *in vitro* reconstituted Syn 1/αSyn condensates with *Scg3* or *Prnp* RNA 25 min of incubation addition of all three components in the reaction mix.

e, Quantifications of αSyn fluorescence intensities in *in vitro* reconstituted Syn 1/*Scg3*/αSyn and Syn 1/*Prnp*/αSyn condensates at two different time points (t1=5 and t2=25 min upon type II reaction set-up). Paired two-tailed T-test comparing the intensities of αSyn within condensates at t1 and t2 result in a P-value of 0.1652 and 0.1633 for conditions containing *Scg3* and *Prnp*, respectively. All the box plots (b, c, e) encompass the 25th and 75th quartiles with the median marked by central line. Whiskers extend to 1.5 times the interquartile range (IQR). Circles indicate outliers. All the data were collected from three independent *in vitro* reconstitutions.

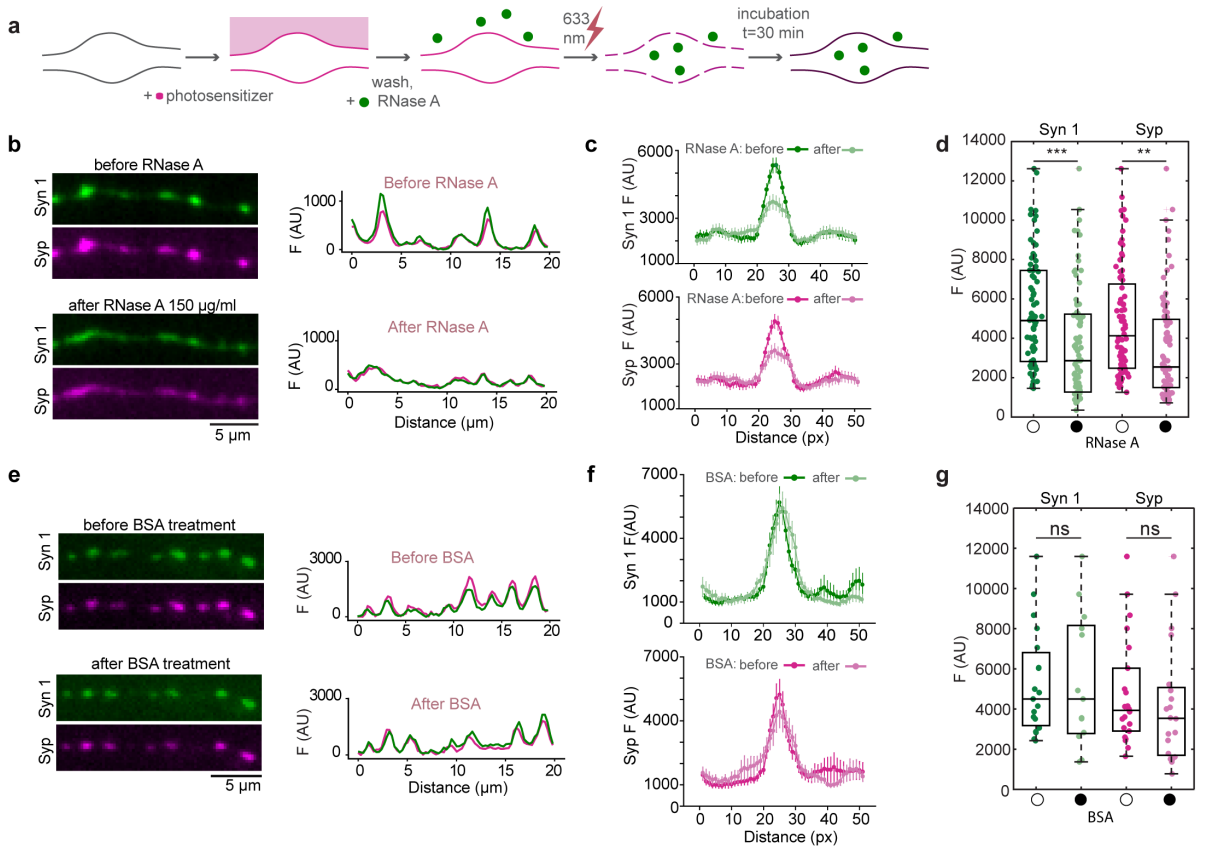

Figure 5 | Acute RNA disruption leads to partial dispersion of synaptic vesicle cluster.
a, Scheme representing a modified photochemical internalization (PCI) method applied for RNase A treatment of rat primary hippocampal neuron culture.
b, Representative micrographs of axon before and after RNase A treatment showing mScarlet-synapsin-1 (Syn 1) and EGFP-synaptophysin (Syp) signal distribution at the synaptic boutons accompanied with the corresponding Syn 1 (green) and Syp (magenta) fluorescence intensity line profiles of representative axon segment. **c,** Averaged intensity line scans of individual boutons representing Syn 1 (above) and Syp (below) fluorescence intensity signal before and after RNase A treatment. Error bars represent standard error of the mean (± SEM). Data was collected from 3 independent primary cultures.
d, Quantifications of Syn 1 and Syp peak fluorescence signal at the synaptic boutons before and after RNase A treatment. The box plot of quantified peak fluorescence signal encompasses 25th and 75th quartiles with median marked by central line. Minimum and maximum are denoted by whiskers. Individual circles represent peak fluorescence signal of a single bouton for each condition. ** indicates $P \leq 0.01$ and *** indicates $P \leq 0.001$ by paired t-test. Data was collected from three independent biological replicates.
e, Representative micrographs of axon before and after BSA treatment showing Syn 1 and Syp signal distribution at the synaptic boutons in the presence of the photosensitizer used for PCI.
f, Averaged intensity line scans of individual boutons representing Syn 1 (left) and Syp (right) fluorescence intensity signal before and after BSA treatment. Error bars represent standard error of the mean (± SEM). Data are from three independent biological replicates.
g, Quantifications of Syn 1 and Syp peak fluorescence signal at the synaptic boutons before and after BSA treatment. The box plot of quantified peak fluorescence signal encompasses 25th and 75th quartiles with median marked by central line. Minimum and maximum are denoted by whiskers. Individual circles represent peak fluorescence signal of a single bouton for each condition. ns indicates non-significant by paired Wilcoxon test. Data were collected from three independent biological replicates.

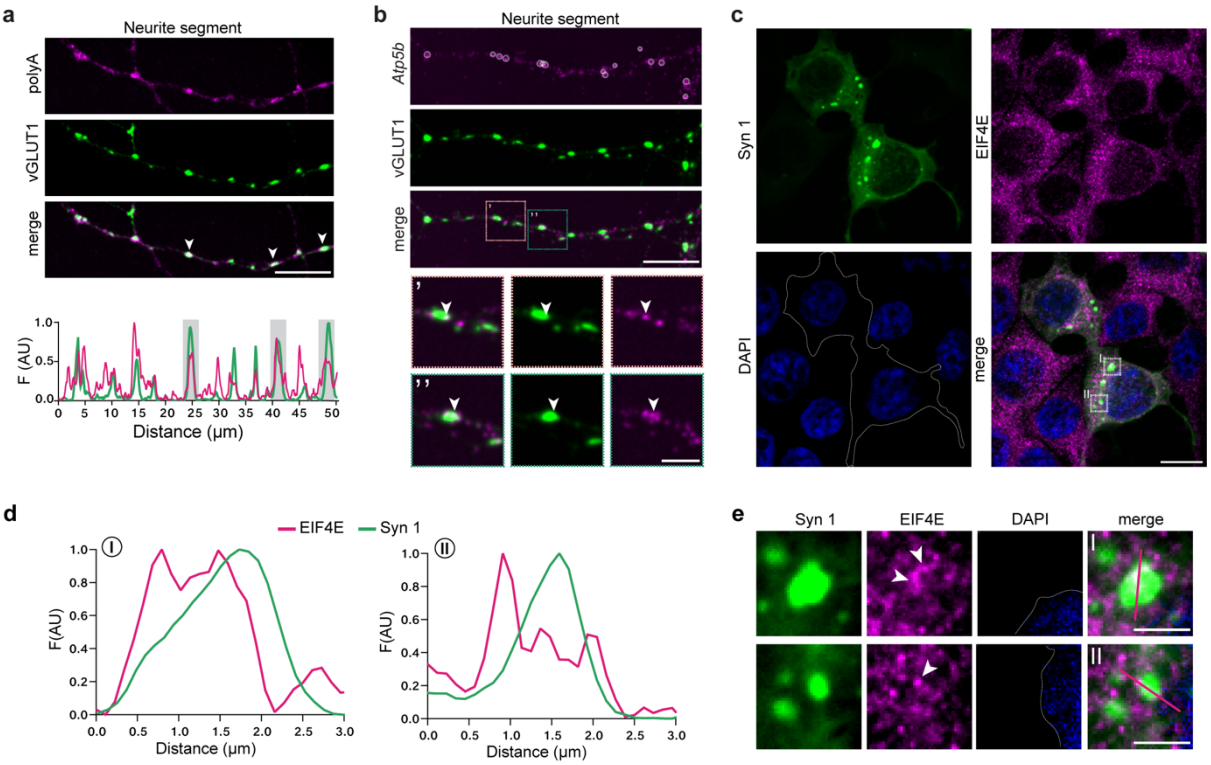

Figure 6 | Synapsin-1 condensates harbor mRNA and the translational machinery components. **a**, Representative images of neurite segment showing poly(A) FISH signal (magenta) and immunostaining against presynaptic marker vGLUT1 (green) in mouse primary hippocampal neurons. Arrows in merge indicate overlap between poly(A) and vGLUT1 in the presynaptic compartment. Bottom: line profiles represent quantified normalized fluorescence intensity signal (F) of poly(A) and vGLUT1 along 50 µm long neurite segment presented in images above. Scale bar: 10 µm.
b, Representative images of neurite segment showing neurite segment with detected *Atp5b* smFISH (magenta) with white circles indicating segmented *Atp5b* foci using RS-FISH analysis software and vGLUT1 signal (green). In merge panels light orange (') and green ('') insets highlight presynaptic region shown in panel below. Scale bar: 10 µm. Arrows indicate *Atp5b* signal co-localizing with vGLUT1. For insets scale bar: 3 µm.
c, HEK293 cells expressing synapsin-1 condensates (mCherry -synapsin-1; Syn 1 in green) fixed and immunostained for EIF4E translational regulator (magenta), DAPI: nucleus. Scale bar, 10 µm.
d, Line profiles across exemplary condensates shown in *e.*
e, Magnified regions of condensates from panel c (white dashed quadrats). Arrows indicate few EIF4E foci. In merge note the accumulation of EIF4E at the interface and within condensates. Gaussian filter (0.4) was applied to magnified insets for better visualization. Dark pink lines in merge (I and II) indicate trajectory of respective fluorescence intensity (F) line profiles in panel d. Scale bars: 3 µm.

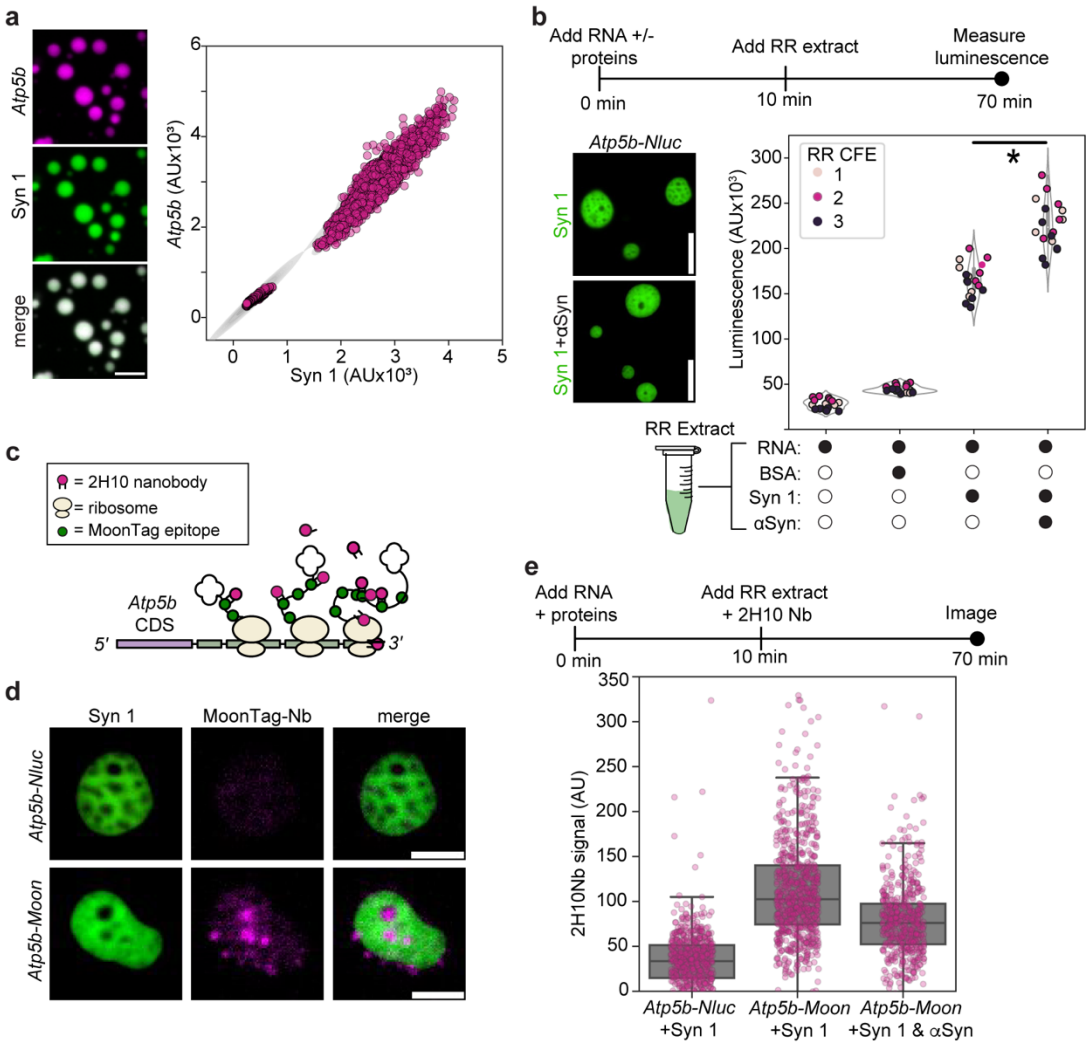

Figure 7 | Synapsin-1 condensates promotes mRNA translation.
a, Left: images showing *Atp5b* synaptic mRNA (magenta) enriching synapsin-1 condensates (Syn 1, green) in *in vitro* system under physiological conditions and in the absence of any molecular crowders. Scale bar: 5 µm. Right: Scatter plot depicts quantified *Atp5b* RNA intensities as a function of Syn 1 intensities. Each circle represents individual condensate analyzed overlaying Kernel Density Estimate (KDE). Data were collected from three independent *in vitro* reconstitutions of *in vitro* transcribed Cy5 labelled *Atp5b* and purified EGFP-tagged synapsin-1.
b, Top: scheme represents simplified overview of the *in vitro* luciferase translation assay using *Atp5b*-nano-luciferase (*Atp5b-Nluc*) as an RNA reporter. Below left: representative images of Syn 1 and synapsin-1/α-synuclein (Syn 1+αSyn) condensates in rabbit reticulocyte extract (RRE). Scale bar: 5 µm. Below right: The violin plot shows quantification of the *Atp5b-Nluc*luminescence signal under different reaction conditions (only *Atp5b-Nluc; Atp5b-Nluc*+ BSA*; Atp5b-Nluc*+ Syn 1*; Atp5b-Nluc* +Syn 1 & αSyn) after incubation in RRE for 60 min. Within each violin plot, the box depicts the 25th through the 75th quartiles, with whiskers extending to min and max data point. The median for each treatment is indicated by a white circle in the center of the violin. Data was collected from three separate RREs (RRE CFE 1-3; see panel legend). Each individual circle represents a technical replicate within that RRE. Below the plot, white circles denote the absence of the reaction component whilst black indicates the inclusion of that reaction component. Paired, two-tailed T-tests were carried out comparing luminescence values in no-Syn 1 conditions to conditions including Syn 1 or Syn 1 + αSyn. Corresponding P-values were <0.00001 and <0.00001 for the no-RNA condition compared to Syn 1 or Syn 1+αSyn, respectively. Additionally, luminescence values of Syn 1 compared against Syn 1 + αSyn conditions yielded a P-value of <0.00001(*).

c, Scheme of MoonTag system developed to quantitatively detect translation events live *in cellulo* and in our work optimized for *in vitro* system of Syn 1 condensates in RR extract.
d, Representative images of Syn 1 (green) and MoonTag(-Nb) nanobody signal (magenta) in condensates enriched with Syn 1 and *Atp5b-Nluc* used as negative control (upper image panel) and *Atp5b-MoonTag* reporter RNA (lower image panel) 60 min after the addition of RRE to pre-formed Syn 1/RNA condensates. Scale bar: 2 µm.
e, Top: schematic overview of the *in vitro* MoonTag translation pipeline in RRE using *Atp5b*-MoonTag (*Atp5b-Moon*) RNA reporter system. Bottom: box plot showing anti-MoonTag nanobody (2H10Nb) fluorescence values for the different *in vitro* conditions (only *Atp5b-Nluc*+Syn 1 [negative control], *Atp5b-Moon*+ Syn 1, *Atp5b-Moon*+ Syn 1+ α-Syn) 60 min after the addition of RRE. For each box plot, the horizontal line in the box plot denote the median value of data distribution between 25th and 75th percentiles. Whiskers extend to 1.5× the IQR. Each magenta circle represents individual condensate analyzed. Data were collected from 3 independent RR extracts. Paired, two-tailed T-tests were carried out comparing mCherry-2H10Nb values between reactions containing *Atp5b-Nluc* and both conditions (*Atp5b-Moon*+Syn 1 and *Atp5b-Moon*+Syn 1+ αSyn; P-values <0.0001, respectively) and between *Atp5b-Moon*+Syn1 and *Atp5b-Moon*+Syn1+aSyn (P-value = 0.001166).

Author contributions

DM, ASG, BR, ZMG designed the study, interpreted results and wrote the initial version of the manuscript. BR, ZMG, AC, CH, AnC, performed *in vitro* reconstitutions and analyzed the data. ZMG and IS designed and *in vitro* transcribed the RNAs used in the study. SR performed and analyzed PCI mediated RNase A assay in neurons. BR and AnC performed condensate purification for RNAseq. KF, MJ, FH and KN helped with the RNA sequencing. VMJ and IS performed RNAseq data analysis and ZMG conducted MEME analysis. AC, CH and GAP performed protein purification. BR performed all FISH and ICC experiments in HEK cells and primary neurons and analyzed the data. ZMG performed and analyzed *in vitro* translation assays. All the authors read and approved the final manuscript.

Acknowledgements

We thank Advanced Medical Bioimaging Core Facility (AMBIO) at Charité University Clinic (Berlin, Germany), Flow Cytometry and Genomics Platform at Max-Delbrück-Centrum für Molekulare Medizin | BIMSB (Berlin, Germany) for the support; to Silvio O. Rizzoli (Göttingen) for the advice and guidance for the RNase A treatment analysis in neurons; to Vladimir Despic (Frankfurt) for discussions. The work is supported by the start-up funds from DZNE, the grants from the German Research Foundation (MI 2104 and SFB1286/B10) and the ERC Grant MemLessInterface (101078172) to DM; the HHMI Faculty Scholar Award and National Science Foundation NSF 743900 to ASG. CH is supported by a fellowship of the Innovative Minds Program of the German Dementia Association.

Competing interests. The authors declare no competing financial interests.

Statistics and Reproducibility. The number of biological and technical replicates and the number of analyzed molecules are indicated in the figure legends and Source Data. Statistical tests were performed using R-studio and Prism 9 (Graphpad).

Data Availability. Source data are provided with this paper. All data generated or analyzed for this study are available within the paper and its associated supplementary information files. All other data presented are available upon reasonable request from the corresponding author.

Code Availability. All codes written for this study are available upon reasonable request from the corresponding authors.

686 **References**
687

688 1. Jahn, R., Cafiso, D. C. & Tamm, L. K. Mechanisms of SNARE proteins in membrane
689 fusion. *Nat. Rev. Mol. Cell Biol.* **25**, 101–118 (2024).

690 2. Holt, C. E., Martin, K. C. & Schuman, E. M. Local translation in neurons: visualization
691 and function. *Nat. Struct. Mol. Biol.* **26**, 557–566 (2019).

692 3. Rangaraju, V., Dieck, S. tom & Schuman, E. M. Local translation in neuronal
693 compartments: how local is local? *EMBO Rep.* **18**, 693–711 (2017).

694 4. Ingolia, N. T., Ghaemmaghami, S., Newman, J. R. S. & Weissman, J. S. Genome-Wide
695 Analysis in Vivo of Translation with Nucleotide Resolution Using Ribosome Profiling.
696 *Science* **324**, 218–223 (2009).

697 5. Koltun, B. *et al.* Measuring mRNA translation in neuronal processes and somata by tRNA-
698 FRET. *Nucleic Acids Res.* **48**, e32–e32 (2020).

699 6. Glock, C. *et al.* The translatome of neuronal cell bodies, dendrites, and axons. *Proc. Natl.*
700 *Acad. Sci. USA* **118**, e2113929118 (2021).

701 7. Dieterich, D. C. *et al.* In situ visualization and dynamics of newly synthesized proteins in
702 rat hippocampal neurons. *Nat. Neurosci.* **13**, 897–905 (2010).

703 8. Ifrim, M. F., Williams, K. R. & Bassell, G. J. Single-Molecule Imaging of PSD-95 mRNA
704 Translation in Dendrites and Its Dysregulation in a Mouse Model of Fragile X Syndrome. *J.*
705 *Neurosci.* **35**, 7116–7130 (2015).

706 9. Giuditta, A., Dettbarn, W. D. & Brzin, M. Protein synthesis in the isolated giant axon of
707 the squid. *Proc. Natl. Acad. Sci. USA* **59**, 1284–7 (1968).

708 10. Giuditta, A. *et al.* Active polysomes in the axoplasm of the squid giant axon. *J. Neurosci.*
709 *Res.* **28**, 18–28 (1991).

710 11. Cajigas, I. J. *et al.* The Local Transcriptome in the Synaptic Neuropil Revealed by Deep
711 Sequencing and High-Resolution Imaging. *Neuron* **74**, 453–466 (2012).

712 12. Shigeoka, T. *et al.* Dynamic Axonal Translation in Developing and Mature Visual
713 Circuits. *Cell* **166**, 181–192 (2016).

714 13. Younts, T. J. *et al.* Presynaptic Protein Synthesis Is Required for Long-Term Plasticity of
715 GABA Release. *Neuron* **92**, 479–492 (2016).

716 14. Hafner, A.-S., Donlin-Asp, P. G., Leitch, B., Herzog, E. & Schuman, E. M. Local protein
717 synthesis is a ubiquitous feature of neuronal pre- and postsynaptic compartments. *Science*
718 **364**, (2019).

719 15. Biever, A. *et al.* Monosomes actively translate synaptic mRNAs in neuronal processes.
720 *Science* **367**, (2020).

721 16. Yao, J., Sasaki, Y., Wen, Z., Bassell, G. J. & Zheng, J. Q. An essential role for β-actin
722 mRNA localization and translation in Ca2+-dependent growth cone guidance. *Nat. Neurosci.*
723 **9**, 1265–1273 (2006).

724 17. Gracias, N. G., Shirkey-Son, N. J. & Hengst, U. Local translation of TC10 is required for
725 membrane expansion during axon outgrowth. *Nat. Commun.* **5**, 3506 (2014).

726 18. Cioni, J.-M. *et al.* Late Endosomes Act as mRNA Translation Platforms and Sustain
727 Mitochondria in Axons. *Cell* **176**, 56-72.e15 (2019).

728 19. Liao, Y.-C. *et al.* RNA Granules Hitchhike on Lysosomes for Long-Distance Transport,
729 Using Annexin A11 as a Molecular Tether. *Cell* **179**, 147-164.e20 (2019).

730 20. Banani, S. F., Lee, H. O., Hyman, A. A. & Rosen, M. K. Biomolecular condensates:
731 organizers of cellular biochemistry. *Nat. Rev. Mol. Cell. Biol.* **18**, 285 298 (2017).

732 21. Corbet, G. A. & Parker, R. RNP Granule Formation: Lessons from P-Bodies and Stress
733 Granules. *Cold Spring Harb. Symp. Quant. Biol.* **84**, 040329 (2020).

734 22. Besse, F. & Ephrussi, A. Translational control of localized mRNAs: restricting protein
735 synthesis in space and time. *Nat. Rev. Mol. Cell Biol.* **9**, 971–980 (2008).

736 23. Liao, G., Mingle, L., Water, L. V. D. & Liu, G. Control of cell migration through mRNA
737 localization and local translation. *RNA* **6**, 1–15 (2015).

738 24. Glock, C., Heumüller, M. & Schuman, E. M. mRNA transport & local translation in
739 neurons. *Curr. Opin. Neurobiol.* **45**, 169–177 (2017).

740 25. Han, T. W. *et al.* Cell-free formation of RNA granules: bound RNAs identify features and
741 components of cellular assemblies. *Cell* **149**, 768 779 (2012).

742 26. Molliex, A. *et al.* Phase separation by low complexity domains promotes stress granule
743 assembly and drives pathological fibrillization. *Cell* **163**, 123 133 (2015).

744 27. Maharana, S. *et al.* RNA buffers the phase separation behavior of prion-like RNA binding
745 proteins. *Science* **360**, 918–921 (2018).

746 28. Fernandopulle, M. S., Lippincott-Schwartz, J. & Ward, M. E. RNA transport and local
747 translation in neurodevelopmental and neurodegenerative disease. *Nat. Neurosci.* **24**, 622–
748 632 (2021).

749 29. Milicevic, K., Rankovic, B., Andjus, P. R., Bataveljic, D. & Milovanovic, D. Emerging
750 Roles for Phase Separation of RNA-Binding Proteins in Cellular Pathology of ALS.
751 *Frontiers Cell Dev. Biol.* **10**, 840256 (2022).

752 30. Sansevrino, R., Hoffmann, C. & Milovanovic, D. Condensate biology of synaptic vesicle
753 clusters. *Trends Neurosci* (2023) doi:10.1016/j.tins.2023.01.001.

754 31. Clemson, C. M. *et al.* An Architectural Role for a Nuclear Noncoding RNA: NEAT1
755 RNA Is Essential for the Structure of Paraspeckles. *Mol. Cell* **33**, 717–726 (2009).

32. Grzejda, D. *et al.* The long noncoding RNA mimi scaffolds neuronal granules to maintain nervous system maturity. *Sci. Adv.* **8**, eabo5578 (2022).

33. Ferrandon, D., Koch, I., Westhof, E. & Nüsslein–Volhard, C. RNA–RNA interaction is required for the formation of specific bicoid mRNA 3′ UTR–STAUFEN ribonucleoprotein particles. *EMBO J.* **16**, 1751–1758 (1997).

34. Jambor, H., Brunel, C. & Ephrussi, A. Dimerization of oskar 3′ UTRs promotes hitchhiking for RNA localization in the Drosophila oocyte. *RNA* **17**, 2049–2057 (2011).

35. Langdon, E. M. *et al.* mRNA structure determines specificity of a polyQ-driven phase separation. *Science* **360**, 922–927 (2018).

36. Mateju, D. *et al.* Single-Molecule Imaging Reveals Translation of mRNAs Localized to Stress Granules. *Cell* **183**, 1801-1812.e13 (2020).

37. Chen, R., Stainier, W., Dufourt, J., Lagha, M. & Lehmann, R. Direct observation of translational activation by a ribonucleoprotein granule. *Nat. Cell Biol.* **26**, 1322–1335 (2024).

38. Ramat, A., Haidar, A., Garret, C. & Simonelig, M. Spatial organization of translation and translational repression in two phases of germ granules. *Nat. Commun.* **15**, 8020 (2024).

39. Pathak, J., Priyadarshini, E., Rawat, K. & Bohidar, H. B. Complex coacervation in charge complementary biopolymers: Electrostatic versus surface patch binding. *Adv. Colloid Interface Sci.* **250**, 40–53 (2017).

40. Wilhelm, B. G. *et al.* Composition of isolated synaptic boutons reveals the amounts of vesicle trafficking proteins. *Science* **344**, 1023 1028 (2014).

41. Milovanovic, D., Wu, Y., Bian, X. & Camilli, P. D. A liquid phase of synapsin and lipid vesicles. *Science* **361**, 604 607 (2018).

42. Hoffmann, C. *et al.* Driving forces for condensation of synapsin are governed by sequence-encoded molecular grammars. *bioRxiv* 2024.08.03.606464 (2024) doi:10.1101/2024.08.03.606464.

43. Bose, M., Rankovic, B., Mahamid, J. & Ephrussi, A. An architectural role of specific RNA–RNA interactions in oskar granules. *Nat. Cell Biol.* **26**, 1934–1942 (2024).

44. Boeynaems, S. *et al.* Spontaneous driving forces give rise to protein−RNA condensates with coexisting phases and complex material properties. *Proc. Natl. Acad. Sci. USA* **116**, 7889–7898 (2019).

45. Seim, I. *et al.* RNA encodes physical information. *bioRxiv* 2024.12.11.627970 (2024) doi:10.1101/2024.12.11.627970.

46. Hofacker, I. L. *et al.* Fast folding and comparison of RNA secondary structures. *Monatshefte für Chem. Chem. Mon.* **125**, 167–188 (1994).

47. Lorenz, R. *et al.* ViennaRNA Package 2.0. *Algorithms Mol. Biol.* **6**, 26 (2011).

48. Hoffmann, C. *et al.* Synapsin Condensates Recruit alpha-Synuclein. *J. Mol. Biol.* 166961 (2021) doi:10.1016/j.jmb.2021.166961.

49. Sharma, M. & Burré, J. α-Synuclein in synaptic function and dysfunction. *Trends Neurosci.* **46**, 153–166 (2023).

50. Park, D. *et al.* Cooperative function of synaptophysin and synapsin in the generation of synaptic vesicle-like clusters in non-neuronal cells. *Nat. Commun.* **12**, 263 (2021).

51. Hubstenberger, A. *et al.* P-Body Purification Reveals the Condensation of Repressed mRNA Regulons. *Mol. Cell* **68**, 144-157.e5 (2017).

52. Bailey, T. L. & Elkan, C. Fitting a mixture model by expectation maximization to discover motifs in biopolymers. *Proc. Int. Conf. Intell. Syst. Mol. Biol.* **2**, 28–36 (1994).

53. Todd, A. K., Johnston, M. & Neidle, S. Highly prevalent putative quadruplex sequence motifs in human DNA. *Nucleic Acids Res.* **33**, 2901–2907 (2005).

54. Fay, M. M., Lyons, S. M. & Ivanov, P. RNA G-Quadruplexes in Biology: Principles and Molecular Mechanisms. *J. Mol. Biol.* **429**, 2127–2147 (2017).

55. Muto, Y. *et al.* Single cell transcriptional and chromatin accessibility profiling redefine cellular heterogeneity in the adult human kidney. *Nat. Commun.* **12**, 2190 (2021).

56. Laghmach, R. *et al.* RNA chain length and stoichiometry govern surface tension and stability of protein-RNA condensates. *iScience* **25**, 104105 (2022).

57. Epple, R. *et al.* The Coding and Small Non-coding Hippocampal Synaptic RNAome. *Mol. Neurobiol.* **58**, 2940–2953 (2021).

58. Berg, K. *et al.* Photochemical Internalization: A New Tool for Drug Delivery. *Curr. Pharm. Biotechnol.* **8**, 362–372 (2007).

59. Soe, T. H., Watanabe, K. & Ohtsuki, T. Photoinduced Endosomal Escape Mechanism: A View from Photochemical Internalization Mediated by CPP-Photosensitizer Conjugates. *Molecules* **26**, 36 (2020).

60. Neckelmann, N. *et al.* The human ATP synthase β subunit gene: Sequence analysis, chromosome assignment, and differential expression. *Genomics* **5**, 829–843 (1989).

61. Kügelgen, N. von & Chekulaeva, M. Conservation of a core neurite transcriptome across neuronal types and species. *Wiley Interdiscip. Rev.: RNA* **11**, e1590 (2020).

62. Boersma, S. *et al.* Multi-Color Single-Molecule Imaging Uncovers Extensive Heterogeneity in mRNA Decoding. *Cell* **178**, 458-472.e19 (2019).

63. Ray, D. *et al.* RNA-binding proteins that lack canonical RNA-binding domains are rarely sequence-specific. *Sci. Rep.* **13**, 5238 (2023).

824 64. Hoffmann, C. *et al.* Synapsin condensation controls synaptic vesicle sequestering and
825 dynamics. *Nat. Commun.* **14**, 6730 (2023).

826 65. Hallacli, E. *et al.* The Parkinson's disease protein alpha-synuclein is a modulator of
827 processing bodies and mRNA stability. *Cell* **185**, 2035-2056.e33 (2022).

828 66. Sahadevan, S. *et al.* Synaptic FUS accumulation triggers early misregulation of synaptic
829 RNAs in a mouse model of ALS. *Nat. Commun.* **12**, 3027 (2021).

830 67. Kumar, S. *et al.* Synaptosome microRNAs regulate synapse functions in Alzheimer's
831 disease. *npj Genom. Med.* **7**, 47 (2022).

832 68. Steward, O. & Levy, W. Preferential localization of polyribosomes under the base of
833 dendritic spines in granule cells of the dentate gyrus. *J. Neurosci.* **2**, 284–291 (1982).

834 69. Yoon, B. C. *et al.* Local Translation of Extranuclear Lamin B Promotes Axon
835 Maintenance. *Cell* **148**, 752–764 (2012).

836 70. Wong, H. H.-W., Watt, A. J. & Sjöström, P. J. Synapse-specific burst coding sustained by
837 local axonal translation. *Neuron* **112**, 264-276.e6 (2024).

838 71. Riggs, C. L., Kedersha, N., Ivanov, P. & Anderson, P. Mammalian stress granules and P
839 bodies at a glance. *J. Cell Sci.* **133**, jcs242487 (2020).

840 72. Riback, J. A. *et al.* Stress-Triggered Phase Separation Is an Adaptive, Evolutionarily
841 Tuned Response. *Cell* **168**, 1028-1040.e19 (2017).

842 73. Tsang, B. *et al.* Phosphoregulated FMRP phase separation models activity-dependent
843 translation through bidirectional control of mRNA granule formation. *Proc National Acad Sci*
844 **116**, 4218–4227 (2019).

845 74. Hoffmann, C. *et al.* Electric Potential at the Interface of Membraneless Organelles
846 Gauged by Graphene. *Nano Lett.* (2023) doi:10.1021/acs.nanolett.3c02915.

847 75. Dai, Y. *et al.* Interface of biomolecular condensates modulates redox reactions. *Chem* **9**,
848 1594–1609 (2023).

849 76. Farag, M. *et al.* Condensates formed by prion-like low-complexity domains have small-
850 world network structures and interfaces defined by expanded conformations. *Nat. Commun.*
851 **13**, 7722 (2022).